Quantum confinement and interference via Fabry-Pérot-like resonators in rhombohedral trilayer graphene on graphite

Zi-Yi Han,[1,2] Lin He,[2] and Long-Jing Yin[1,3,*]

[1]*Key Laboratory for Micro/Nano Optoelectronic Devices of Ministry of Education & Hunan Provincial Key Laboratory of Low-Dimensional Structural Physics and Devices, School of Physics and Electronics, Hunan University, Changsha 410082, China*

[2]*Center for Advanced Quantum Studies, Department of Physics, Beijing Normal University, Beijing 100875, China*

[3]*Research Institute of Hunan University in Chongqing, Chongqing 401120, China*

(Received 27 June 2023; revised 13 November 2023; accepted 7 December 2023; published 21 December 2023)

Rhombohedral trilayer graphene (rTG) has recently emerged as a new playground for exploring flatband-induced exotic quantum phenomena and sparked considerable concern. However, the experimental accessing of local quantum behaviors such as the quantum confinement of flatband electrons in rTG has been highly limited so far. Here, using scanning tunneling microscopy and spectroscopy, we study the quantum confinement and interference of quasiparticles in rTG via Fabry-Pérot-like resonators. The resonators are formed by narrow rTG terraces with different geometries. In a narrow rectangular terrace (∼50-nm width) made by two parallel step edges, we observe quantum confined states, which can be accurately replicated by the Fabry-Pérot model. These confined states are highly governed by the transmission and scattering from the electronic states of adjacent graphene layers, leading to significant broadening and suppression of the flatband peak in rTG. The effective length of the flatband suppression is determined to be ∼15–30 nm for different step edges. Furthermore, we reveal the quasiparticle interference around two intersecting step edges, whose features can be well simulated by a developed Fabry-Pérot model. These findings not only uncover the fundamental properties of quasiparticle interference in confined rTG systems, but also provide important insight into the interactions between the flatband electrons of rTG and their surrounding environments.

DOI: 10.1103/PhysRevB.108.245422

I. INTRODUCTION

Rhombohedral, or *ABC*-stacked, trilayer graphene has been demonstrated to be an attractive platform due to its inherent possession of nearly flat bands at the charge-neutrality point (CNP) localized around the *K* point of the Brillouin zone [1–8]. Recent transport experiments have revealed that such partially flat bands in rhombohedral trilayer graphene (rTG) can also give rise to a plethora of strongly correlated phases including superconductivity and magnetism [9–11], which bear a striking resemblance to those emerged in magic-angle twisted graphene [12,13]. Furthermore, it has been found that the flatband structure of rTG, as well as the induced correlated electronic states, can be effectively modulated by forming heterostructures with vertically stacked hexagonal boron nitride [14–16]. These exciting related studies establish rTG as a new versatile platform to engineer and investigate strongly correlated flatband physics [17–20]. Despite extensive research, the local quantum properties of rTG have rarely been accessed so far, and no confined flatband states in closed rTG geometries at the nanometer scale have been observed.

In this paper, we use scanning tunneling microscopy and spectroscopy (STM and STS) to investigate the quantum confinement and interference of quasiparticles in rTG nanoscale Fabry-Pérot-like resonators. The Fabry-Pérot-like resonators are realized in narrow rTG terraces with different geometries, which are formed by parallel and intersecting step edges. For the narrow rectangular rTG terrace (∼50-nm width) made by two parallel step edges, our tunneling conductance measurements discover spatially dependent quantum confined states, which can be accurately reproduced by the Fabry-Pérot model. The observed confined states are found to be highly governed by the interactions with the electronic states of adjacent graphene layers, resulting in the increased width and reduced intensity of the flatbands in rTG. Moreover, for the intersecting rTG step edges, we image their typical quasiparticle interference patterns and find that their features can be simulated by a developed Fabry-Pérot model. Our findings offer a microscopic understanding of the confined rTG systems and the interactions between flatband electrons and their surrounding environments.

II. RESULTS AND DISCUSSION

The rTG samples were prepared on highly oriented pyrolytic graphite substrates (HOPG, ZYA grade, from SurfaceNet). The HOPG substrates were surface cleaved by adhesive tape in atmosphere conditions before being rapidly transferred into the ultrahigh-vacuum STM chamber. On the surface-cleaved HOPG substrates, an increase in interlayer spacing or a large rotation between the top few-layer graphene flakes and underlying substrates easily occur due to cleavage, which can generate electronically decoupled graphene flakes on the HOPG surface. This phenomenon has been widely reported in previous experiments [8,21–25]. Our studied rTG

*yinlj@hnu.edu.cn

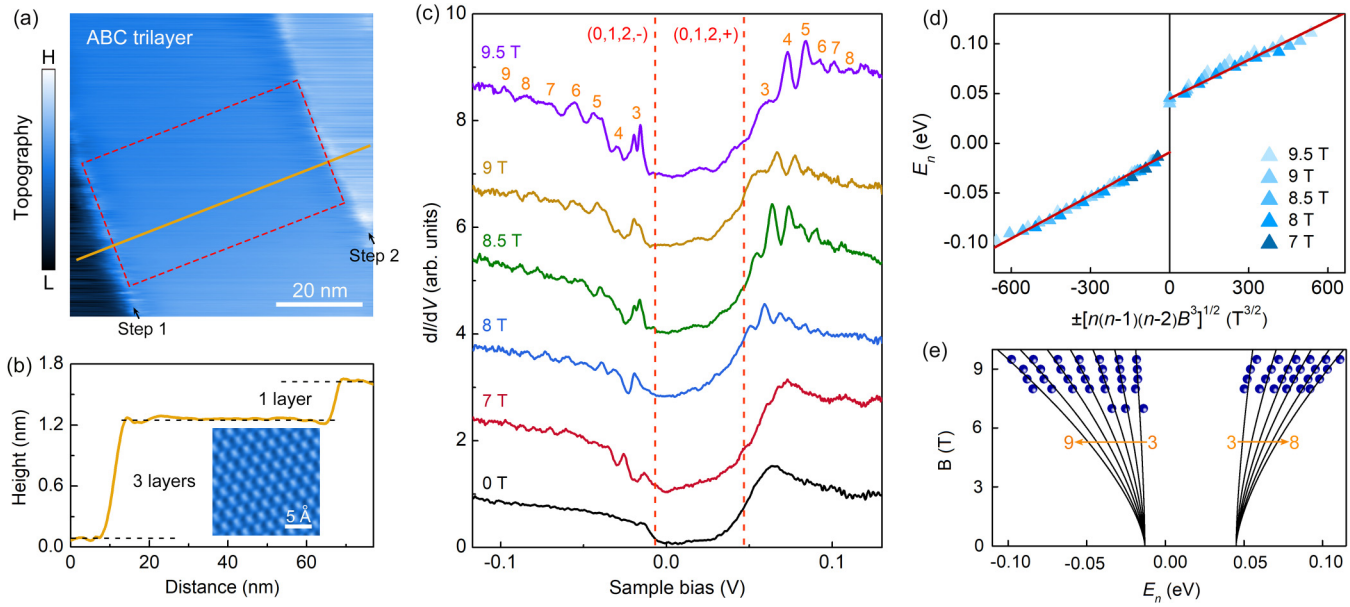

FIG. 1. (a) STM topographic image ($70 \times 70\,\mathrm{nm}^2$, $V_b = 80$ mV, $I = 0.3$ nA) of an *ABC*-stacked trilayer graphene between two adjacent step edges. (b) Height profile of the two step edges along the solid line in (a). The upper one is a one-layer step edge and the lower one is a three-layer step edge. Inset is an atomic-resolution STM image ($V_b = 80$ mV, $I = 0.3$ nA) of the rTG. (c) Typical *dI/dV* spectra ($V_m = 1$ mV) measured under various magnetic fields. Curves are vertically shifted for clarity. LL peaks are labeled by numbers. The LL peaks were determined based on their reproducibility in various spatially resolved spectra (see details in Ref. [26]). (d) Extracted LL peak energies from (c) as a function of $\pm[n(n-1)(n-2)B^3]^{1/2}$. (e) LL fan diagram deduced from (c). The solid curves are fits of the data (dots) with theory. The error of each LL peak energy was obtained from the standard deviation of the peak energies measured from various spectra, with the error bar being smaller than the symbol size.

are naturally existing structures in those electronically decoupled graphene flakes on top of the HOPG. The *ABC* stacking order of the rTG and its decoupling nature were identified by Landau-level (LL) spectroscopy (see details below and in the Supplemental Material, including Figs. S1 and S2 [26]). STM/STS measurements were performed in an ultrahigh-vacuum low-temperature UNISOKU STM system ($\sim 10^{-11}$ Torr, $\sim$4.5 K) with constant-current mode. STM topographic images were calibrated against the standard graphene lattice and the Si(111)-(7×7) lattice using mechanically roughened Pt/Ir tips. STS measurements were carried out by a standard lock-in technique with an AC modulation of 1–5 mV and 793 Hz.

Figure 1(a) shows the STM topographic image of a rTG sample on HOPG substrate. The rTG region is confined within two nearly parallel step edges marked by step 1 and step 2. From the height profile line across the steps [Fig. 1(b)] and the atomic resolution images of the step edges (Fig. S3 [26]), we can deduce that step 1 is a three-layer terminated step edge of the rTG and step 2 corresponds to a step edge of an extra monolayer graphene placed atop the rTG. This configuration results in a narrow rectangular rTG terrace with the width of $\sim$50 nm. Before accessing the confinement effect in this rTG terrace, we first discuss its stacking arrangement and decoupling nature. The rhombohedral stacking order can be efficiently identified through magnetic field-varied STS measurements [Figs. 1(c)–1(e)], as we previously reported in rTG [8,27,28]. Under zero magnetic field, the *dI/dV* spectrum recorded on the rTG terrace displays a band-gap feature near the Fermi energy. For rTG, the substrate and STM tip easily introduce an interlayer electric field and break the inversion symmetry of the rTG, giving rise to a finite energy gap opened at the CNP [21,27,29,30]. At the edge of the conduction band, a density of states (DOS) peak is observed. This DOS peak results from the nearly flat band of rTG residing on the top layer [21,27,29]. In the presence of perpendicular magnetic fields, the STS spectra of the rTG develop into a series of well-defined LL peaks [marked by numbers in Fig. 1(c)] as the magnetic length is much smaller than the width of confined rTG terrace [26]. The theoretical LL sequences of a gapped rTG based on the simplest tight-binding model (only considering nearest-intralayer and interlayer hopping [31,32]) were predicted as $E_n = E_C \pm (2\hbar v_F^2 eB)^{3/2}\sqrt{n(n-1)(n-2)}/\gamma_1^2 \pm E_g/2$, where E_C is the energy of CNP, $\pm$ represents electron and hole, $\hbar$ is Planck's constant, $v_F \sim 10^6$ m/s is the Fermi velocity, e is the electron charge, $n =$ integer is the LL index, γ_1 is the nearest-neighbor interlayer coupling strength, and E_g is the band gap. We extract the energies of the observed LLs from Fig. 1(c) and plot them against $\pm[n(n-1)(n-2)B^3]^{1/2}$ and B in Figs. 1(d) and 1(e), respectively. The experimental data fit well with the theoretical LL sequences, yielding $E_g \approx 55$ meV and $\gamma_1 \approx 0.56$ eV which both agree well with early experiments [5,8,21,27,28,33] and theory [1]. The well-defined characteristic of the LLs and their good agreement with theory shown in Figs. 1(c)–1(e) demonstrate unambiguously that this sample is an *ABC*-stacked trilayer graphene which is electronically decoupled from the HOPG substrate. We note that the step height of this rTG ($\sim 1.12 \pm 0.05$ nm) is measured to be slightly larger than the normal value of three

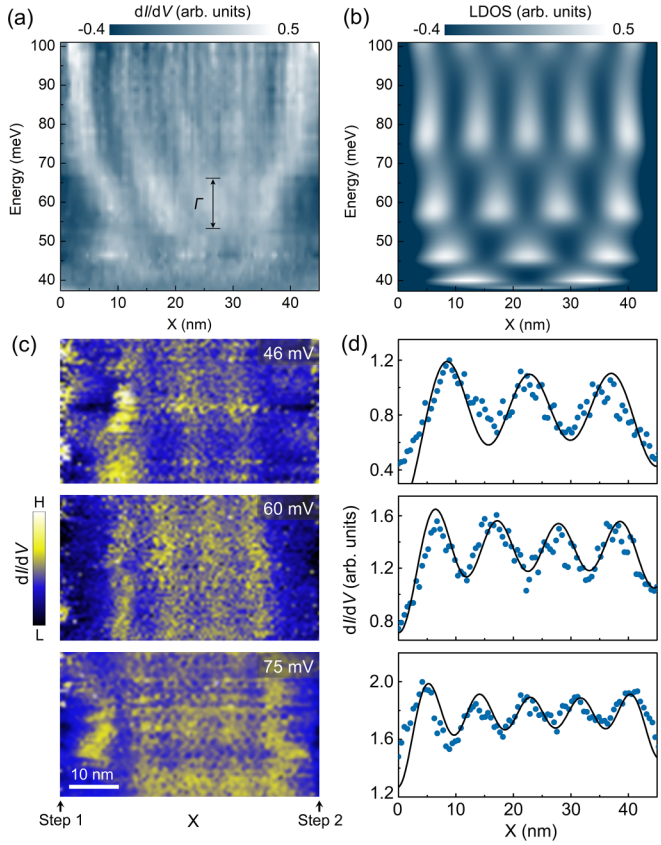

FIG. 2. (a) Spatially resolved contour plot of *dI/dV* spectra (V_m = 1 mV) across the rTG resonator from step 1 to step 2 in Fig. 1(a). (b) Calculated LDOS of the studied rTG resonator using Fabry-Pérot model. (c) *dI/dV* maps of the red dashed square area in Fig. 1(a) at 46, 60, and 75 meV. (d) Corresponding averaged *dI/dV* line cuts across the two steps for the STS maps in (c). Each of the data is averaged from a dozen *dI/dV* line cuts obtained throughout the STS maps. The solid curves are Fabry-Pérot model fits to the data (dots). $r_1 = 0.52$, $r_2 = 0.22$ (46 meV); $r_1 = 0.47$, $r_2 = 0.17$ (60 meV); $r_1 = 0.37$, and $r_2 = 0.2$ (75 meV).

graphene layers (∼1.02 nm), suggesting an increased interlayer spacing-induced decoupling origin for this rTG.

The nanoscale rTG terrace confined within two parallel step edges shown in Fig. 1 offers an unprecedented platform for exploring quantum confinement effect of the flatband electrons in rTG. Figure 2(a) shows a spatially resolved contour plot of *dI/dV* spectra near the conduction-band edge (e.g., the nearly flat-band states) measured across the rTG terrace from step 1 to step 2. Obvious standing-wave patterns are visualized in the whole map, together with the signature of quantized resonance states at the energies of ∼45, ∼60, and ∼75 meV. To clearly reveal the quantized resonance states, we performed energy-fixed *dI/dV* mapping at these specific energies, as shown in Fig. 2(c). The quantized resonances are evident in the conductance maps as well as in their spatially averaged *dI/dV* line cuts [Fig. 2(d)]. The observed standing-wave patterns and the quantized resonance states are caused by scattering and interference of the rTG quasiparticles confined within nanoscale-separated step edges, which resembles the behavior of a Fabry-Pérot resonator. The Fabry-Pérot resonator or interferometer is known in optics and is made by partially reflecting mirrors with the reflection coefficient r and reflection phase ϕ. In our case, the reflection phases at step 1 and step 2 can be set as $\phi = -\pi$, and the reflection coefficients are set to an identical r in the beginning. Therefore, based on the Fabry-Pérot model, the local DOS ρ_s of the rTG quasiparticles in the resonator can be expressed as [34,35]

$$\rho_s(E,x) = \rho_b + \frac{2L_0}{\pi}\int_0^k dq \frac{1-r^2}{\sqrt{k^2-q^2}} \times \frac{1+r^2+r(\cos[2q(x-a)+\pi]+\cos[2qx-\pi])}{1+r^4-2r^2\cos[2qa-2\pi]},$$

where $k = \pm\sqrt[3]{\gamma_1^2(E-E_C)/(v_F\hbar)^3}$, $L_0 = m^*/(\pi\hbar^2)$ is the DOS of a free 2D electron with $m^* = 0.05\, m_e$ extracted from experiment of multilayer graphene [26,36], and a is the width of the resonator. The energy of the CNP $E_C = 37$ meV and the nearest-neighbor interlayer hopping strength $\gamma_1 = 0.56$ eV have been determined above. Besides, ρ_b is used as an independent fit parameter that describes an offset likely related to transmission across the step edges or scattering into the graphite bulk. It varies between 0.4–1.4 L_0 and increases with energy, but does not affect the fitting of reflection coefficients [35]. Figure 2(b) shows the simulated results for our rTG resonator using the above Fabry-Pérot model. The simulation nicely reproduces the main experimental features observed in Fig. 2(a).

With a close examination of the resonance electronic states observed experimentally in Fig. 2, we can find an asymmetric amplitude of the standing waves between the two step edges. As shown in Fig. 2(d), the amplitudes of the resonance peaks at step 1 side are slightly larger than that at step 2 side, indicating an asymmetric resonator model. To further uncover the local quantum behaviors of rTG quasiparticles confined in our resonator, we conducted an asymmetric Fabry-Pérot resonator simulation by utilizing unequal reflection coefficients (r_1 and r_2) for the two steps. An excellent agreement between the measured resonance states and the asymmetric resonator model is obtained as shown in Fig. 2(d). From this asymmetric model fitting within various energies, we obtained the reflection coefficients $r_1 \approx 0.5$ and $r_1 \approx 0.28$ for step 1 and step 2, respectively [see detailed values for different energies in Fig. 3(a)]. The reflection coefficients exhibit relatively small values, which are comparable to those measured in step resonators of noble-metal surface states [34], topological surface states [37], and heavy fermion systems [38]. The small reflection amplitudes strongly suggest the existence of quasiparticle scattering between the rTG and its surroundings, such as the substrate and extra graphene layer. The quasiparticle scattering into the surroundings also can be evidenced by examining the energy broadening (Γ) of the resonant levels (i.e., the inverse lifetime of quasiparticles). As shown in Fig. 3(b), the extracted Γ exhibits a nearly E^2 energy dependence (see Fig. S4 for details of the extraction of Γ), indicating clear electron-electron scattering similar to the case in topological insulators [37] and 2D heavy fermions [38]. It is worth noting that previous studies on metal surfaces [34,39] have

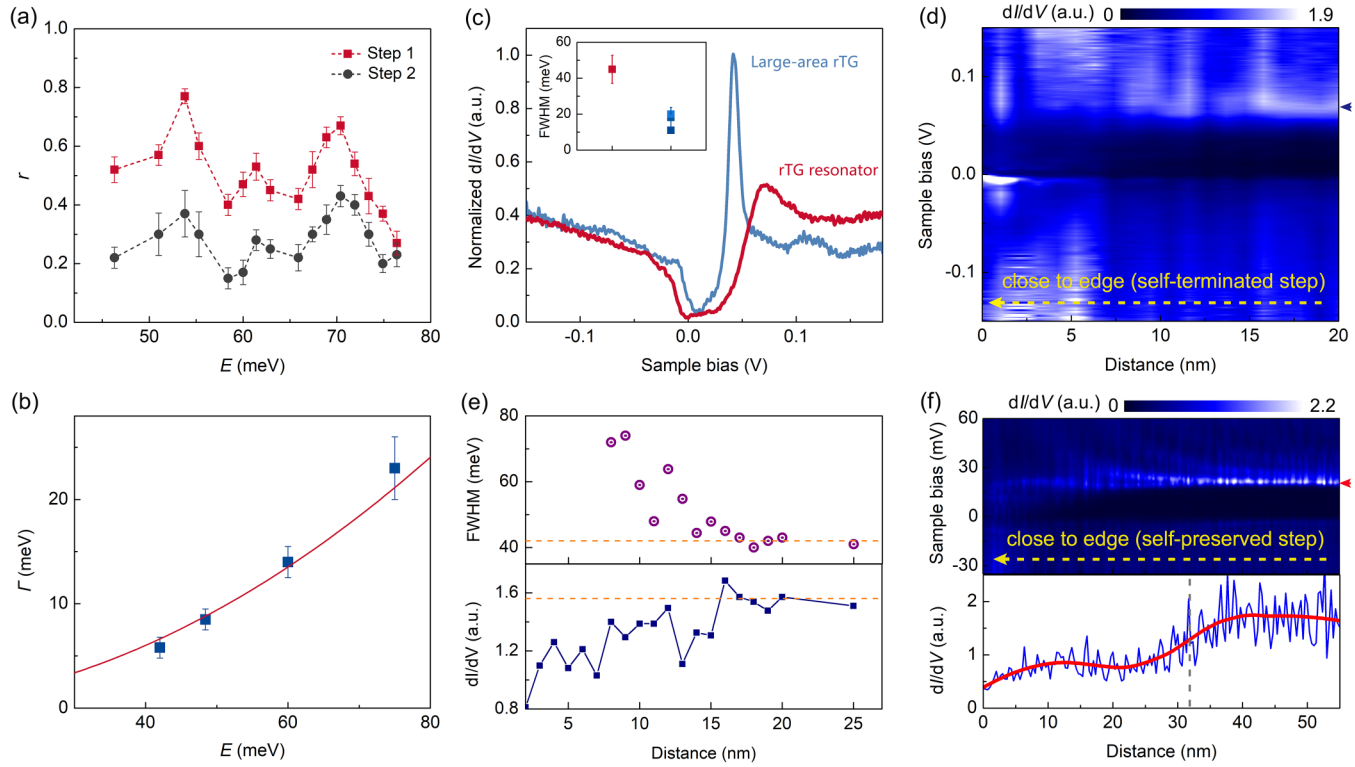

FIG. 3. (a) Reflection amplitudes for the two step edges of the rTG resonator deduced from the Fabry-Pérot model. (b) Energy broadening of the resonant levels shown in Fig. 2(a). The data (squares) are obtained by measuring the FWHM of the resonant peaks from Gaussian fit. The red curve is a parabolic fit. (c) Normalized zero-field *dI/dV* spectra measured in the middle region of the studied rTG resonator (red curve) and on another rTG sample with a large terrace (blue curve). Inset shows the FWHM of flatband peak extracted from the rTG resonator (red square) and other rTG samples with large terraces (blue squares). (d) Spatially resolved *dI/dV* contour plot near the edge of step 1. (e) Spatial evolution of the flatband width (upper panel) and height (lower panel) extracted from (d). Dashed lines denote the average values of the flatband width and height away from the edge. (f) Upper panel: spatially resolved STS contour plot near the self-preserved step edge of a large-area rTG. Lower panel: *dI/dV* line cut (blue curve) along the flatband peak energy (marked by arrow in upper panel). The red line is the smoothing result of the data. $V_m = 1$ mV for all *dI/dV* spectra.

demonstrated a decrease in reflection amplitudes as energy increases, which has also been attributed to the coupling between surface and bulk states. In our experiment, the reflection amplitude for step 1 exhibits a decreasing trend with increasing energy, while no discernible energy dependence is observed for step 2. Besides, the reflection coefficient of step 1 is nearly a factor of 2 larger than that of step 2. This difference arises from the geometrical origin: the extra step (step 2) presents a relatively soft barrier compared to the intrinsic step (step 1), similar to that observed on Ag(111) surface [34].

To investigate the origin of the extra quasiparticle scattering in the rTG resonator and its influence on the flatband electrons, we measured the STS spectra on other rTG samples with large terraces (hundreds of nanometers size) on HOPG substrate and compared them to the studied rTG resonator. The results are depicted in Fig. 3(c). Compared to that in large rTG terraces, the DOS peak of the nearly flat bands in the rTG resonator exhibits significant broadening. The measured full width at half maximum (FWHM) of the flatband peak is ∼45 meV for the rTG resonator (away from the edges) and ∼11–20 meV for those large-area rTG [inset of Fig. 3(c)]. Besides, the intensity of the flatband peak in the rTG resonator is also much weaker than that in unconfined rTG. The substantial broadening and suppression of the flatband peak indicate that the flatband electronic states in the step-type rTG resonator suffer a strong scattering with those non-flatband states. It should be noted that the large-area rTG samples used for comparison were deliberately chosen for their highly similar configurations to the confined rTG, specifically having comparable gap size and interlayer spacing with the substrate (see Fig. S5 for details [26]). Thus, the scattering induced by direct coupling with the substrate electronic states is expected to demonstrate comparable strength in both types of rTG samples. This indicates that the rTG resonator possesses additional scattering channels. The most probable scattering channel is from the step edges [34]. In the step-type rTG resonator, the presence of step edges facilitates mixing between rTG states and their orthogonal substrate and extra-layer states, resulting in the additional and strong scattering effects.

The step-edge induced strong scattering can be evidenced by the position-dependent STS spectra near step edges. As shown in Figs. 3(d) and 3(e), the flatband peak is further suppressed and broadened as it approaches the edge of step 1. The suppression range near the edge is ∼15 nm, considering both the weakening and broadening effects on the flatband peak (Fig. 3(e) and Fig. S6 [26]). Similar result is also observed near the same step-type edge in a large rTG terrace (see

Fig. S7 [26]). The above suppression range is smaller than the size of our rTG resonator, but it is only the effect of the step-1 type edge—the self-terminated step edge where the graphene layers are all terminated. We thus investigate the length scale of flatband peak suppression for the step-2 type edge, i.e., the self-preserved step edge where the graphene layers are (all or partly) preserved. To avoid the limitation of the sample size, we measured the flatband peak suppression near the self-preserved step edge in a large rTG terrace. A suppression length exceeding 30 nm is obtained from the second type of edge (Fig. 3(f), and see Fig. S8 for details [26]). This length is approximately twice as large as that for the self-terminated step edge and exceeds the half-width of our rTG resonator. Therefore, the two different step edges (step 1 and step 2) jointly induce strong scattering effects almost throughout the entire range of our resonator, resulting in the significant suppression of the flatbands. The much longer suppression length observed at the self-preserved step edge, compared with the self-terminated step edge, strongly indicates the presence of substantial electronic transmission across the steps due to its partial layer continuity. This long-range transmission has been found at analogous atomic steps in a topological insulator with comparable length scale [37]. However, the observed flatband suppression length of up to 30 nm is not yet understood and requires further quantitative investigation. We deduce that the electronic transmission effect is also responsible for the notably low reflection coefficients obtained at step 2 [Fig. 3(a)]. Our observed significant transmission and scattering through steps thus emphasizes the influence of geometrical morphology and surrounding environments on the flatband electronic states.

Next, we investigate the quasiparticle interference near the intersecting rTG step edges. Figure 4(a) shows a STM topographic image of two intersecting step edges (labeled by step 1′ and step 2′) acquired on another rTG sample (see Supplemental Material for details of this sample [26]). The energy-fixed STS mapping recorded over the two intersecting step edges displays complex standing-wave patterns and quantized resonances. As shown in Fig. 4(b) for the STS map at −16 meV, both step edges generate long-range standing waves which overlapped with each other in the rTG terrace, resulting in the discrete resonances. Below we will show that these discrete resonances can also be described by the Fabry-Pérot model. In the Fabry-Pérot resonator made by two parallel reflectors, when the crests and valleys of the standing waves from the two reflectors align, respectively, quantized resonances will emerge at specific energies. For the intersecting reflectors of Fig. 4(b), the two sets of standing waves exhibit an intersecting behavior, generating a network of resonances in real space. To capture the characteristic of the resonance network, we define the peak index of the standing waves as m and n for step 1′ and step 2′, respectively. Subsequently, we can simulate the resonance network of Fig. 4(b), as shown in Fig. 4(c). It can be found that the resonance peaks with the same value of $m + n$ exhibit the same amplitude; see Fig. 4(d) as an example for the dI/dV line cuts along those resonance peaks with $m + n = 8$, 10, and 12 (see more data in the Supplemental Material [26]). This replicates the model of Fabry-Pérot resonances in the parallel reflectors, where resonances are formed by the overlapping of the standing waves with equal sum of peak indices. Therefore, the resonator made by the intersecting step edges can be seen as a Fabry-Pérot resonator with a varying width.

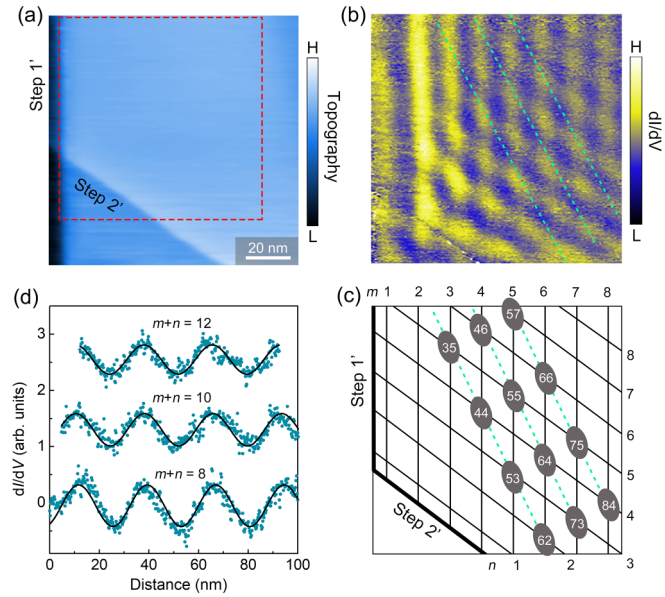

FIG. 4. (a) STM topographic image ($120 \times 120\,\mathrm{nm}^2$, $V_b = 0.15$ V, $I = 0.2$ nA) of another rTG with two intersecting step edges. (b) Spectroscopic map of the red dashed square area in (a) at −16 meV. (c) Schematic of quasiparticle interference measured in (b). m and n define the standing-wave index for step 1′ and 2′, respectively. The green dashed lines connect those resonance peaks with $m + n = 8$, 10, and 12, respectively. (d) LDOS oscillation line cuts along the dashed lines in (b) for $m + n = 8$, 10, and 12. The solid curves are cosine-wave fits to the data (dots), showing constant amplitudes, respectively.

III. SUMMARY

In summary, via STM and STS measurements, we have studied the quantum confinement and interference of quasiparticles in rTG parallel-step type and intersecting-step type nanoscale resonators. Quantized resonances have been visualized in both types of resonators. We found that the observed quantum confined states in the parallel-step type resonator, which can be nicely replicated by the typical Fabry-Pérot model, are profoundly influenced by the transmission and scattering from adjacent graphene layers. This leads to the significant broadening and suppression of the flatbands in rTG over a wide range. Moreover, we imaged resonance network in the intersecting-step type rTG resonator and demonstrated that it can be well described by a developed Fabry-Pérot model. These results provide microscopic insight into the local quantum behaviors in confined rTG systems, emphasizing the influence of surrounding environments on flatbands.

ACKNOWLEDGMENTS

This work was supported by the National Natural Science Foundation of China (Grants No. 12174095, No. 12141401, and No. 11974050) and the Natural Science Foundation of Hunan Province, China (Grant No. 2021JJ20026). L.-J.Y. also acknowledges support from the Science and Technol-

ogy Innovation Program of Hunan Province, China (Grant No. 2021RC3037) and the Natural Science Foundation of Chongqing, China (Grant No. cstc2021jcyj-msxmX0381). The authors acknowledge the financial support from the Fundamental Research Funds for the Central Universities of China.

[1] F. Zhang, B. Sahu, H. Min, and A. H. MacDonald, Band structure of ABC-stacked graphene trilayers, Phys. Rev. B **82**, 035409 (2010).

[2] R. Olsen, R. van Gelderen, and C. M. Smith, Ferromagnetism in ABC-stacked trilayer graphene, Phys. Rev. B **87**, 115414 (2013).

[3] H. Wang, J.-H. Gao, and F.-C. Zhang, Flat band electrons and interactions in rhombohedral trilayer graphene, Phys. Rev. B **87**, 155116 (2013).

[4] W. Bao, L. Jing, J. Velasco, Y. Lee, G. Liu, D. Tran, B. Standley, M. Aykol, S. B. Cronin, D. Smirnov, M. Koshino, E. McCann, M. Bockrath, and C. N. Lau, Stacking-dependent band gap and quantum transport in trilayer graphene, Nat. Phys. **7**, 948 (2011).

[5] L. Zhang, Y. Zhang, J. Camacho, M. Khodas, and I. Zaliznyak, The experimental observation of quantum Hall effect of $l = 3$ chiral quasiparticles in trilayer graphene, Nat. Phys. **7**, 953 (2011).

[6] Y. Lee, D. Tran, K. Myhro, J. Velasco, N. Gillgren, C. N. Lau, Y. Barlas, J. M. Poumirol, D. Smirnov, and F. Guinea, Competition between spontaneous symmetry breaking and single-particle gaps in trilayer graphene, Nat. Commun. **5**, 5656 (2014).

[7] R. Xu, L.-J. Yin, J.-B. Qiao, K.-K. Bai, J.-C. Nie, and L. He, Direct probing of the stacking order and electronic spectrum of rhombohedral trilayer graphene with scanning tunneling microscopy, Phys. Rev. B **91**, 035410 (2015).

[8] L.-J. Yin, L.-J. Shi, S.-Y. Li, Y. Zhang, Z.-H. Guo, and L. He, High-magnetic-field tunneling spectra of ABC-stacked trilayer graphene on graphite, Phys. Rev. Lett. **122**, 146802 (2019).

[9] H. Zhou, T. Xie, T. Taniguchi, K. Watanabe, and A. F. Young, Superconductivity in rhombohedral trilayer graphene, Nature (London) **598**, 434 (2021).

[10] H. Zhou, T. Xie, A. Ghazaryan, T. Holder, J. R. Ehrets, E. M. Spanton, T. Taniguchi, K. Watanabe, E. Berg, M. Serbyn, and A. F. Young, Half- and quarter-metals in rhombohedral trilayer graphene, Nature (London) **598**, 429 (2021).

[11] Y. Lee, S. Che, J. Velasco, Jr., X. Gao, Y. Shi, D. Tran, J. Baima, F. Mauri, M. Calandra, M. Bockrath, and C. N. Lau, Gate-tunable magnetism and giant magnetoresistance in suspended rhombohedral-stacked few-layer graphene, Nano Lett. **22**, 5094 (2022).

[12] Y. Cao, V. Fatemi, S. Fang, K. Watanabe, T. Taniguchi, E. Kaxiras, and P. Jarillo-Herrero, Unconventional superconductivity in magic-angle graphene superlattices, Nature (London) **556**, 43 (2018).

[13] A. L. Sharpe, E. J. Fox, A. W. Barnard, J. Finney, K. Watanabe, T. Taniguchi, M. A. Kastner, and D. Goldhaber-Gordon, Emergent ferromagnetism near three-quarters filling in twisted bilayer graphene, Science **365**, 605 (2019).

[14] G. Chen, A. L. Sharpe, P. Gallagher, I. T. Rosen, E. J. Fox, L. Jiang, B. Lyu, H. Li, K. Watanabe, T. Taniguchi, J. Jung, Z. Shi, D. Goldhaber-Gordon, Y. Zhang, and F. Wang, Signatures of tunable superconductivity in a trilayer graphene moiré superlattice, Nature (London) **572**, 215 (2019).

[15] G. Chen, L. Jiang, S. Wu, B. Lyu, H. Li, B. L. Chittari, K. Watanabe, T. Taniguchi, Z. Shi, J. Jung, Y. Zhang, and F. Wang, Evidence of a gate-tunable Mott insulator in a trilayer graphene moiré superlattice, Nat. Phys. **15**, 237 (2019).

[16] J. Yang, G. Chen, T. Han, Q. Zhang, Y.-H. Zhang, L. Jiang, B. Lyu, H. Li, K. Watanabe, T. Taniguchi, Z. Shi, T. Senthil, Y. Zhang, F. Wang, and L. Ju, Spectroscopy signatures of electron correlations in a trilayer graphene/hBN moiré superlattice, Science **375**, 1295 (2022).

[17] G. Chen, A. L. Sharpe, E. J. Fox, Y. H. Zhang, S. Wang, L. Jiang, B. Lyu, H. Li, K. Watanabe, T. Taniguchi, Z. Shi, T. Senthil, D. Goldhaber-Gordon, Y. Zhang, and F. Wang, Tunable correlated Chern insulator and ferromagnetism in a moiré superlattice, Nature (London) **579**, 56 (2020).

[18] B. L. Chittari, G. Chen, Y. Zhang, F. Wang, and J. Jung, Gate-tunable topological flat bands in trilayer graphene boron-nitride moiré superlattices, Phys. Rev. Lett. **122**, 016401 (2019).

[19] Y. Z. Chou, F. Wu, J. D. Sau, and S. Das Sarma, Acoustic-phonon-mediated superconductivity in rhombohedral trilayer graphene, Phys. Rev. Lett. **127**, 187001 (2021).

[20] Y.-H. Zhang, D. Mao, Y. Cao, P. Jarillo-Herrero, and T. Senthil, Nearly flat Chern bands in moiré superlattices, Phys. Rev. B **99**, 075127 (2019).

[21] L.-J. Yin, L.-Z. Yang, L. Zhang, Q. Wu, X. Fu, L.-H. Tong, G. Yang, Y. Tian, L. Zhang, and Z. Qin, Imaging of nearly flat band induced atomic-scale negative differential conductivity in ABC-stacked trilayer graphene, Phys. Rev. B **102**, 241403(R) (2020).

[22] L.-J. Yin, S.-Y. Li, J.-B. Qiao, J.-C. Nie, and L. He, Landau quantization in graphene monolayer, Bernal bilayer, and Bernal trilayer on graphite surface, Phys. Rev. B **91**, 115405 (2015).

[23] L.-J. Yin, H. Jiang, J.-B. Qiao, and L. He, Direct imaging of topological edge states at a bilayer graphene domain wall, Nat. Commun. **7**, 11760 (2016).

[24] G. Li, A. Luican, and E. Y. Andrei, Scanning tunneling spectroscopy of graphene on graphite, Phys. Rev. Lett. **102**, 176804 (2009).

[25] L.-H. Tong, Q. Tong, L.-Z. Yang, Y.-Y. Zhou, Q. Wu, Y. Tian, L. Zhang, L. Zhang, Z. Qin, and L.-J. Yin, Spectroscopic visualization of flat bands in magic-angle twisted monolayer-bilayer graphene: Coexistence of localization and delocalization, Phys. Rev. Lett. **128**, 126401 (2022).

[26] See Supplemental Material at http://link.aps.org/supplemental/10.1103/PhysRevB.108.245422 for more experimental data and analysis.

[27] L.-J. Yin, Y.-Y. Zhou, L.-H. Tong, L.-J. Shi, Z. Qin, and L. He, Imaging Friedel oscillations in rhombohedral trilayer graphene, Phys. Rev. B **107**, L041404 (2023).

[28] L.-J. Yin, W.-X. Wang, Y. Zhang, Y.-Y. Ou, H.-T. Zhang, C.-Y. Shen, and L. He, Observation of chirality transition of quasiparticles at stacking solitons in trilayer graphene, Phys. Rev. B **95**, 081402(R) (2017).

[29] Y.-P. Wang, X.-G. Li, J. N. Fry, and H.-P. Cheng, First-principles studies of electric field effects on the electronic

structure of trilayer graphene, Phys. Rev. B **94**, 165428 (2016).

[30] M. Yankowitz, J. I. Wang, A. G. Birdwell, Y. A. Chen, K. Watanabe, T. Taniguchi, P. Jacquod, P. San-Jose, P. Jarillo-Herrero, and B. J. LeRoy, Electric field control of soliton motion and stacking in trilayer graphene, Nat. Mater. **13**, 786 (2014).

[31] M. Koshino and E. McCann, Trigonal warping and Berry's phase Nπ in ABC-stacked multilayer graphene, Phys. Rev. B **80**, 165409 (2009).

[32] S. Yuan, R. Roldán, and M. I. Katsnelson, Landau level spectrum of ABA- and ABC-stacked trilayer graphene, Phys. Rev. B **84**, 125455 (2011).

[33] M. Yankowitz, F. Wang, C. N. Lau, and B. J. LeRoy, Local spectroscopy of the electrically tunable band gap in trilayer graphene, Phys. Rev. B **87**, 165102 (2013).

[34] L. Bürgi, O. Jeandupeux, A. Hirstein, H. Brune, and K. Kern, Confinement of surface state electrons in Fabry-Pérot resonators, Phys. Rev. Lett. **81**, 5370 (1998).

[35] K. Chang, B. J. Miller, H. Yang, H. Lin, S. S. P. Parkin, S. Barraza-Lopez, Q.-K. Xue, X. Chen, and S.-H. Ji, Standing waves induced by valley-mismatched domains in ferroelectric SnTe monolayers, Phys. Rev. Lett. **122**, 206402 (2019).

[36] M. Koshino and T. Ando, Orbital diamagnetism in multilayer graphenes: Systematic study with the effective mass approximation, Phys. Rev. B **76**, 085425 (2007).

[37] J. Seo, P. Roushan, H. Beidenkopf, Y. S. Hor, R. J. Cava, and A. Yazdani, Transmission of topological surface states through surface barriers, Nature (London) **466**, 343 (2010).

[38] E. Herrera, I. Guillamon, V. Barrena, W. J. Herrera, J. A. Galvis, A. L. Yeyati, J. Rusz, P. M. Oppeneer, G. Knebel, J. P. Brison, J. Flouquet, D. Aoki, and H. Suderow, Quantum-well states at the surface of a heavy-fermion superconductor, Nature (London) **616**, 465 (2023).

[39] G. Hormandinger and J. B. Pendry, Interaction of surface states with rows of adsorbed atoms and other one-dimensional scatterers, Phys. Rev. B **50**, 18607 (1994).